Electronic Supplementary Information

Hybridization of MXene and covalent organic frameworks as electroactive materials for Li-S batteries and oxygen electrocatalysis

Zhuangzhuang Wu [a,1], Yuzhen Zhao [a,1], Yongpeng Li [b], Xinxin Yu [a], Zhuyin Sui [b,*], Lijuan Feng [c,*], Qi Chen [a,*]

[a] *School of Marine Science and Engineering, State Key Laboratory of Marine Resource Utilization in South China Sea, Hainan University, Haikou, 570228, P.R. China. E-mail: chenqi@hainanu.edu.cn*

[b] *School of Chemistry and Chemical Engineering, Yantai University, Yantai, 264005, P.R. China. E-mail: suizy@ytu.edu.cn*

[c] *School of Bioengineering, Zhuhai Campus of Zunyi Medical University, Zhuhai, 519041, P.R. China. E-mail: fljcyczh@126.com*

* Corresponding Author

[1] These authors contributed equally to this work

Chemicals and reagents

Concretely, 1,3,5-triformylphloroglucinol (Tp, 98.0%) and 2,5-diaminobenzonitrile (Db, 98.0%) were provided from Yanshen Tech. Co. Ltd., Jilin, P. R. China. Ti_3AlC_2 was bought from Xfnano materials Tech. Co. Ltd., Jiangsu, P. R. China. Lithium fluoride (LiF, 99.9%), (3-aminopropyl)triethoxysilane (APTES, 99.0%), 1-methyl-2-pyrrolidinone (NMP, 99.0%), polyvinylidene fluoride (PVDF), 1,3-dioxolane (99.8%), dimethoxymethane (98.0%), sublimed sulfur (98.0%), lithium bis(trifluoromethane)sulfonimide (99.9%), lithium nitrate ($LiNO_3$, 99.0%), iron(II) acetate anhydrous ($Fe(OAc)_2$, 95.0%), cobalt(II) acetate tetrahydrate ($Co(OAc)_2{\cdot}4H_2O$, 99.5%), nickel(II) acetate tetrahydrate ($Ni(OAc)_2{\cdot}4H_2O$, 99.0%), ruthenium(IV) oxide (RuO_2, 99.9%), triethylamine (Et_3N, 99.0%), and hydroxylamine hydrochloride ($NH_2OH{\cdot}HCl$, 99.9%) were obtained from Macklin Biochemical Co. Ltd., Shanghai, P. R. China. Mesitylene (97.0%), 1,4-dioxane (99.0%), hydrochloric acid (HCl, 36.5%), acetic acid (HOAc, 99.5%), tetrahydrofuran (THF, 99.5%), anhydrous ethanol (EtOH, 99.5%), and anhydrous methanol (MeOH, 99.7%) were acquired from Xilong Scientific Co. Ltd., Guangdong, P. R. China. Ultrapure water (UPW, 18.2 MΩ cm) was used in the whole experiment.

Characterizations

The crystalline structure, pore properties, microscopic morphology, and chemical composition of the as-prepared samples were characterized through powder X-ray diffraction (PXRD, Bruker AXS D8, Germany), field-emission scanning electron

microscopy (FE-SEM, JEOL JSM-7500F, Japan), high-resolution transmission electron microscopy (HR-TEM, Thermo Scientific Talos F200i S/TEM, The United States), Fourier transform infrared spectroscopy (FT-IR, PerkinElmer Spectrum Two, The United States), thermal gravimetric analyzer (TGA, PerkinElmer SAT 8000, The United States), X-ray photoelectron spectroscopy (XPS, Thermo Scientific ESCALAB 250Xi, The United States), inductively coupled plasma optical emission spectrometry (ICP-OES, Thermo Scientific iCAP 7400, The United States), and N_2 adsorption-desorption (Micromeritics ASAP 2460, The United States), respectively.

Synthesis of COF-TpDb

Generally, Tp (21.0 mg, 0.10 mmol) and Db (20.0 mg, 0.15 mmol) were dissolved in mesitylene/1,4-dioxane (volume ratio 1:1) mixed solvent in a custom Pyrex tube. This mixture was adequately dispersed via ultrasound, followed by adding 0.2 mL of acetic acid (6 M). After performing three cycles of freezing-vacuum-thawing, the Pyrex tube was sealed through a flamethrower and then kept at 120 °C for 5 d. Finally, the resulting precipitate was purified by means of filtration and soxhlet extraction to obtain the COF-TpDb (Fig. S1). [S1]

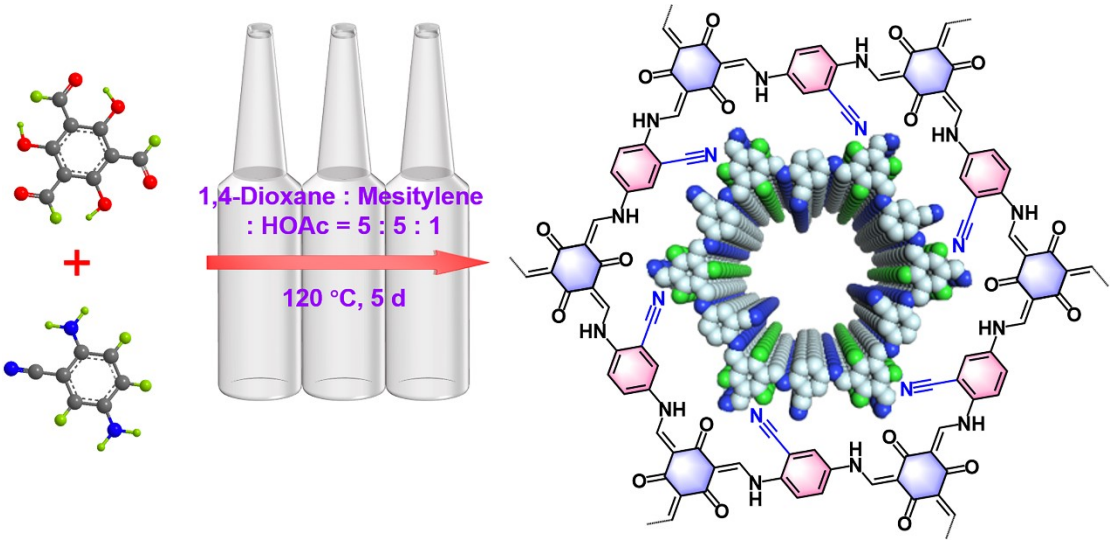

Fig. S1. Scheme diagram for the preparation of COF-TpDb.

Preparation of S-COF-TpDb

S-COF-TpDb was obtained by a sulfur melting and diffusing method. In brief, COF-TpDb and sublimed sulfur (mass ratio 2:3) were completely mixed in a Teflon container, after which they were heated at 155 °C for 12 h to get S-COF-TpDb (Fig. S2).

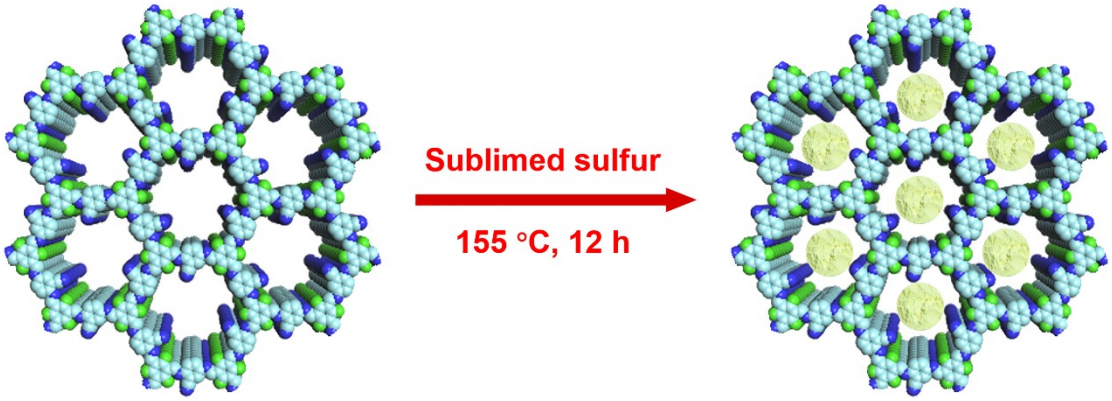

Fig. S2. S-COF-TpDb synthesis method.

Fabrication of S-MX@COF-TpDb

S-MX@COF-TpDb is acquired through a process similar to S-COF-TpDb (Fig. S3).

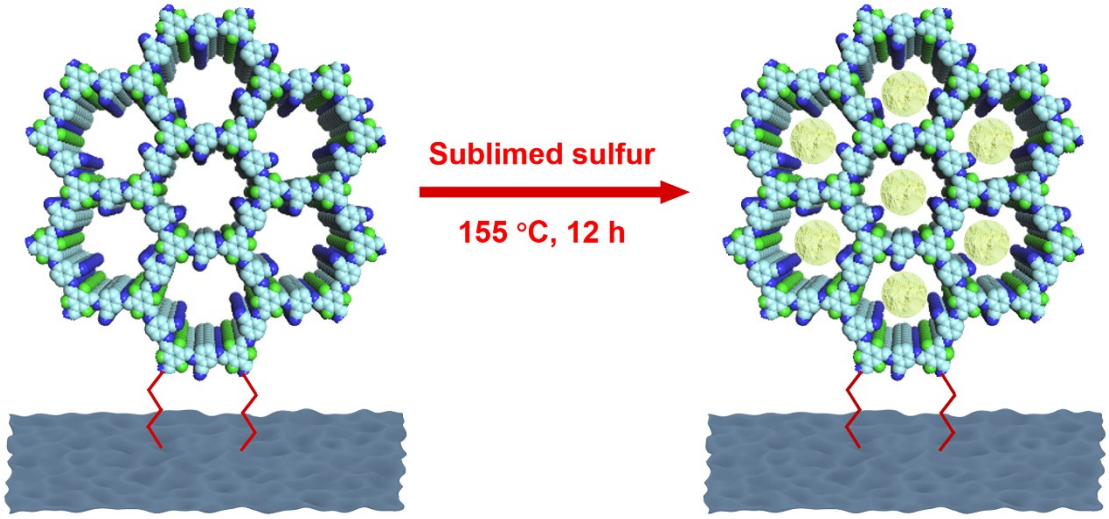

Fig. S3. S-MX@COF-TpDb synthesis method.

Synthesis of S-MXene

The preparation process of S-MXene is similar to that of S-COF-TpDb.

Assembly of Li-S battery

The as-fabricated cathode slurry containing 80 wt % active material (S-MX@COF-TpDb, S-COF-TpDb or S-MXene), 10 wt % polyvinylidene fluoride, and 10 wt % carbon black, was coated onto a carbon-coated aluminum foil and dried at 50 °C for 6 h in a vacuum oven. The CR2032 coin cells were assembled with Li-anode, S-cathode, separator, and electrolyte in an inert gas-filled glovebox, where the moisture and oxygen levels were both kept below 1.0 ppm. The electrolyte was obtained via adding 1.0 wt% $LiNO_3$ into 1.0 M lithium bis(trifluoromethane)sulfonimide salt solution (dimethoxymethane/1,3-dioxolane, 1:1 by volume). The electrolyte/sulfur ratio is around 25 μL mg^{-1} per cell. The active material loading is 1.5−2.0 mg cm^{-2}.

Performance test of Li-S batteries

All Li-S battery experiments were operated through the CR2032 coin cell system. Before testing, the cells were aged for 24 h. Cyclic voltammogram (CV) and electrochemical impedance spectroscopy (EIS) were recorded by electrochemical workstation (CHI760E, Shanghai Chenhua). Discharge-charge performance of different functional materials was tested at the 2001 A.L Land battery. Rate and cycling performance tests on a Neware battery cycler.

Lithium-ion diffusion coefficient

Lithium-ion diffusion coefficient D_{Li^+} ($cm^2\ s^{-1}$) is investigated by cyclic voltammetry method and calculated according to the Randles-Sevick equation:

$$I_p = 269000 \times n^{1.5} \times A \times D_{Li^+}^{0.5} \times C_{Li^+} \times v^{0.5}$$

where I_p is the peak current value (A), n represents the number of electrons of in the reaction (n = 2), A indicates the electrode area (1.13 cm^2), C_{Li^+} means the lithium-ion concentration in the electrolyte (mol mL^{-1}), and v stands for the scanning rate (V s^{-1}).

Synthesis of electrocatalytic OER working electrode

According to the traditional synthesis of catalyst ink, 5 mg of each catalyst was blended with 1 mL of mixed solvent containing 95% ethanol and 5% Nafion, after which it was dispersed by ultrasound for 30 min. Subsequently, 20 μL of catalyst ink was completely dripped onto the glassy carbon working electrode (GCE), followed by drying at ambient environment. Notably, the surface area of GCE is 0.1964 cm^{-2}.

Performance test of electrocatalytic OER

All electrocatalytic OER measurements were carried out on a Ivium CompactStat.h electrochemical workstation with a standard three-electrode system. Among them, 1.0 M KOH aqueous solution, graphite rod electrode, Hg/HgO electrode, and GCE were used as electrolyte, counter electrode, reference electrode, and working electrode, respectively. All measured potentials were converted to the reversible hydrogen electrode (RHE). The overpotential (η) was calculated by $\eta = E_{RHE} - 1.23$.

Before the electrochemical measurements, the working electrode was activated by subjecting to 20 CV cycles in the potential range of 1.22−1.72 V vs. RHE with a scan rate of 100 mV s^{-1}. On this basis, the polarization curves of all catalysts were acquired by linear sweep voltammetry (LSV) at a scan rate of 5 mV s^{-1}. The EIS measurements were performed in frequency ranges from 10 kHz to 0.01 Hz at an overpotential of 349 mV. The electrochemical surface area (ECSA) of Fe/Co-MX@COF-TpDb-AO was estimated by measuring the capacitance of the double layer (C_{dl}) with CV. The C_{dl} was collected through linearly fitting the current density plots at the same potential (1.30 V vs. RHE) with different scan rates from 20 to 100 mV s^{-1}. The turnover frequency (TOF) was calculated by TOF = (J x A)/ (4 x F x n), in which J (mA cm^{-2}) is the current density at a given overpotential, A (cm^2) is the surface area of the electrode, F stands for the Faraday constant (96,485 C mol^{-1}), and n (mol) is the total molar amount of cobalt and iron loaded on the working electrode which was determined via the XPS analysis. Finally, the stability of Fe/Co-MX@COF-TpDb-AO was evaluated by an

accelerated durability test (ADT), which cycled the potential from 1.22 to 1.72 V vs. RHE at 100 mV s^{-1} for 1000 cycles.

Preparation of electrocatalytic ORR working electrode

The three-electrodes were composed of Pt-wire counter electrode, Hg/HgO reference electrode, and glassy-carbon-based working electrode. The electrocatalytic ORR working electrode was prepared as follows: first, a catalyst ink was prepared by ultrasonicating a mixture of 5.0 mg COF-based catalyst without adding any conductive carbon materials, and 1 mL Nafion (0.25 wt%) ethanol solution for 30 min. Subsequently, 15 μL catalyst ink was pipetted onto the GCE surface. Finally, the GCE was dried under an infrared lamp for 3 min. Among them, the surface area of the rotating ring disk electrode is 0.2475 cm^{-2}.

Performance test of electrocatalytic ORR

The ORR activity of various COF-based samples was evaluated under continuous oxygen flow in a 0.1 M KOH aqueous solution as the electrolyte using an electrochemical workstation (Pine AFMSRCE, USA). In addition, the catalysts were operated at 1600 rpm during polarization curve testing, while at 900 rpm during stability testing. In order to illustrate the production rate of the peroxide intermediates and ORR electron transfer mechanism, the rotating ring-disk electrode (RRDE) tests were conducted. The electron transfer numbers (n) were calculated via $n = 4I_D/ (I_D + (I_R/N))$, and the H_2O_2 yields were calculated through $H_2O_2(\%) = (200I_R/N)/ (I_D + (I_R/N))$.

where I_R is the absolute values of the ring current, I_D is the absolute values of the disk current, and $N = 0.37$ is the current collection efficiency at the Pt ring electrode. At last, the accelerated durability tests (ADT) of the Co-MX@COF-TpDb-AO was conducted in O_2-saturated 0.1 M KOH through the chronoamperometric method for 40,000 s at 0.6 V vs. RHE.

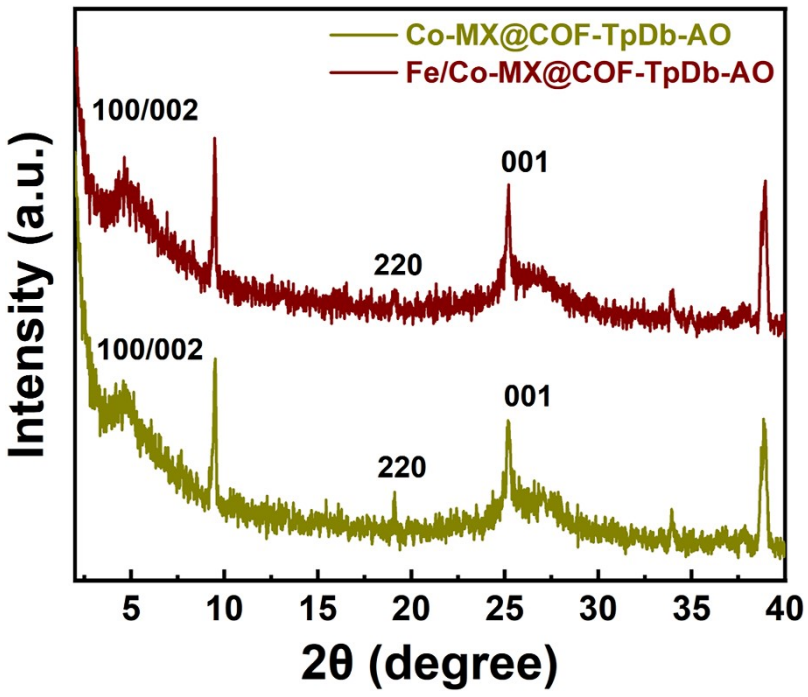

Fig. S4. PXRD profiles of Co-MX@COF-TpDb-AO and Fe/Co-MX@COF-TpDb-AO.

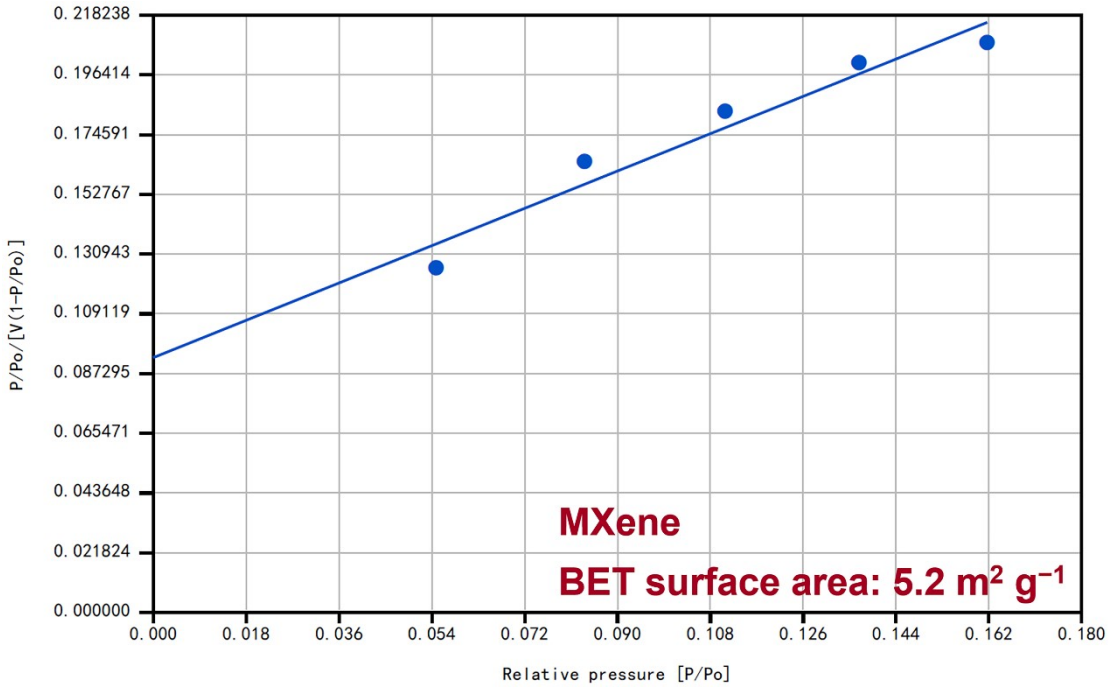

Fig. S5. BET surface area plots of MXene.

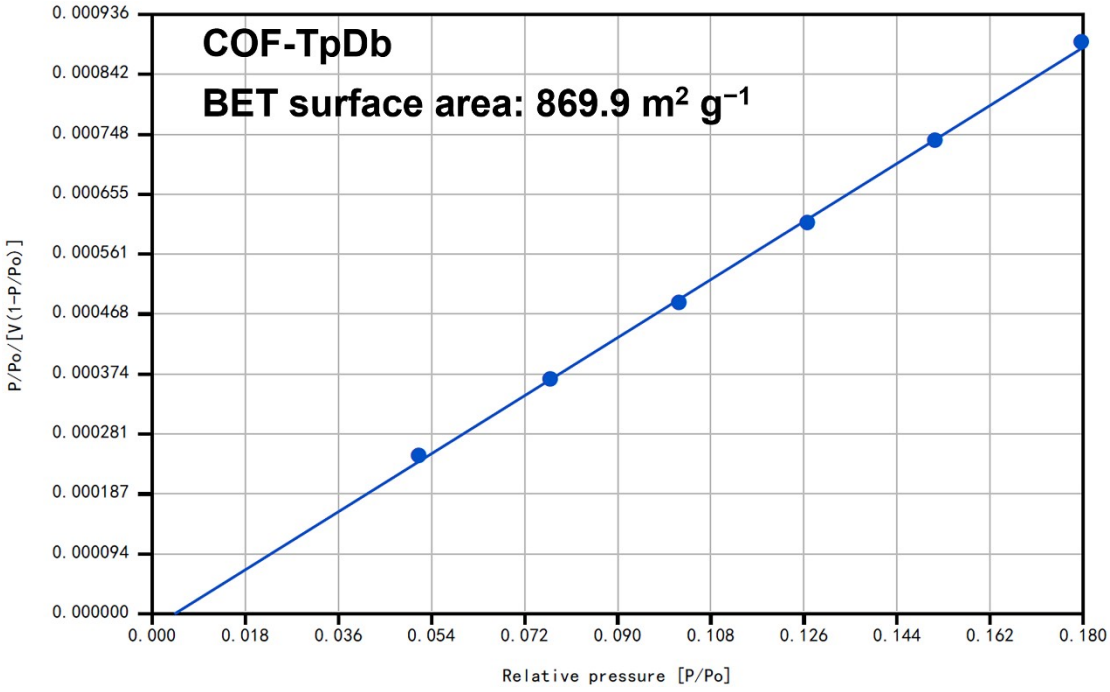

Fig. S6. BET surface area plots of COF-TpDb.

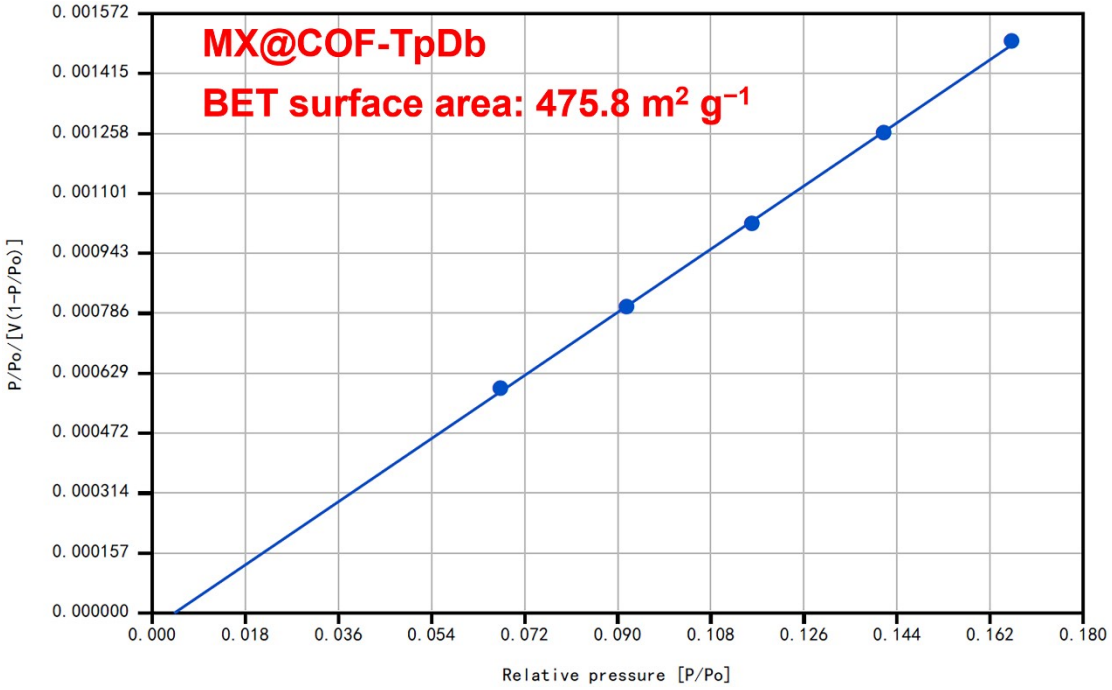

Fig. S7. BET surface area plots of MX@COF-TpDb.

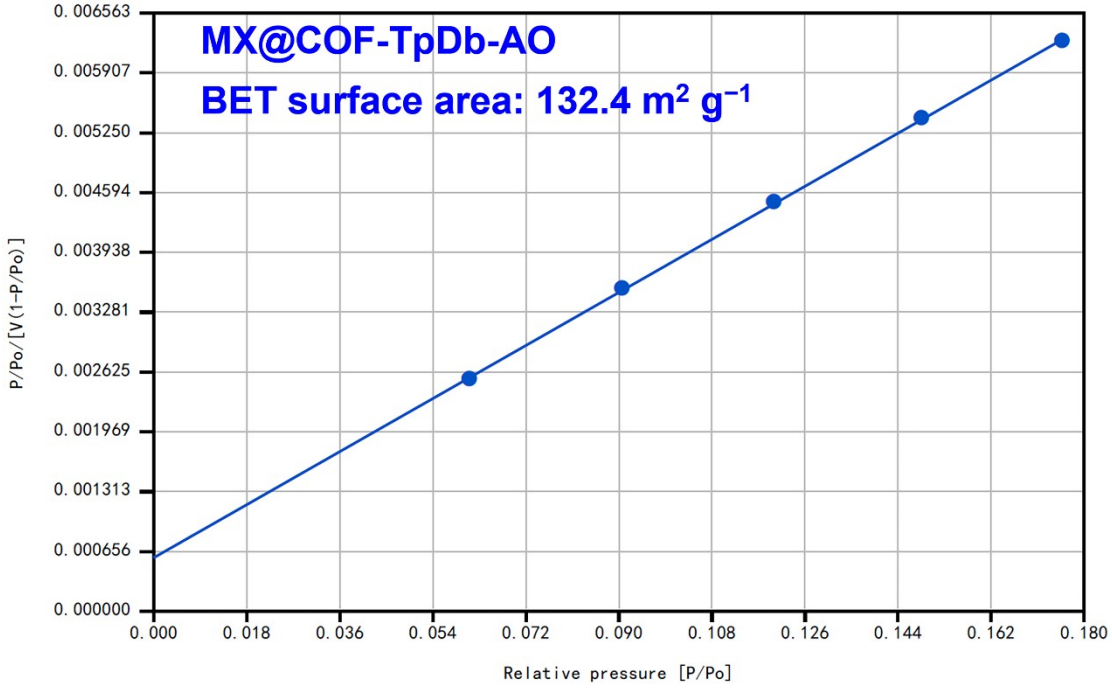

Fig. S8. BET surface area plots of MX@COF-TpDb-AO.

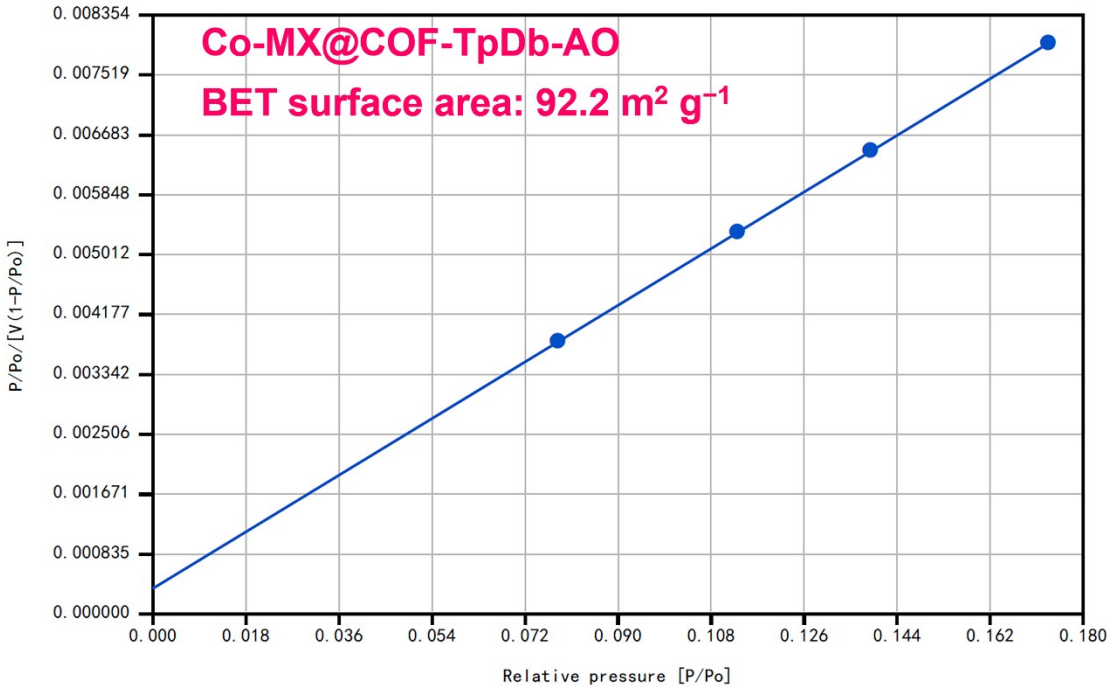

Fig. S9. BET surface area plots of Co-MX@COF-TpDb-AO.

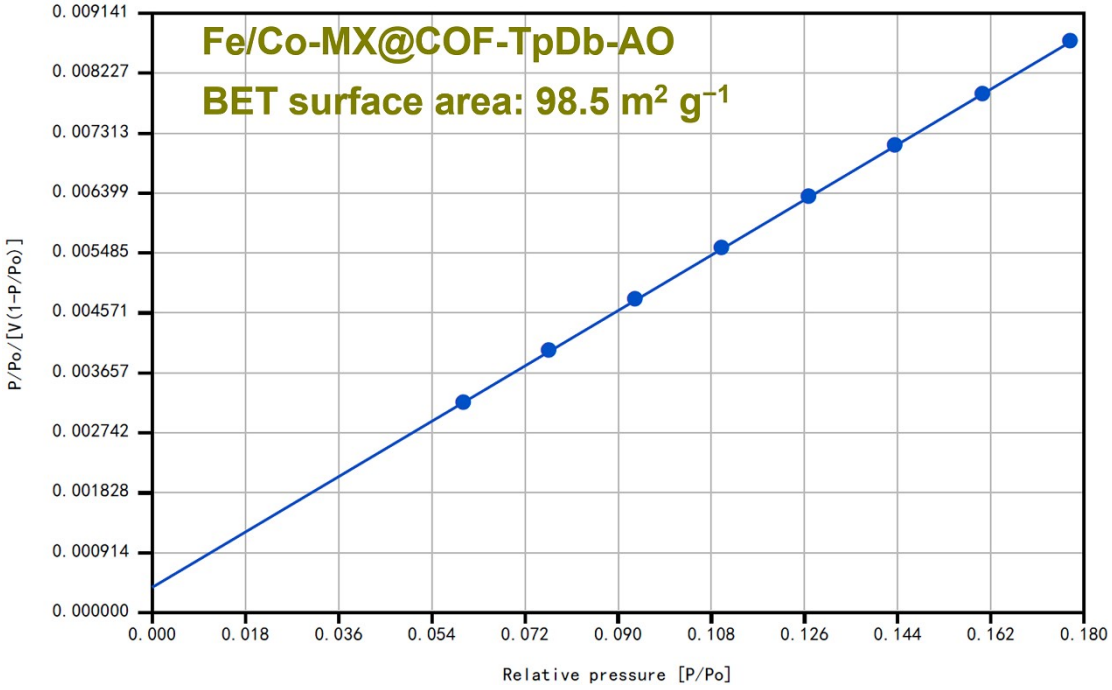

Fig. S10. BET surface area plots of Fe/Co-MX@COF-TpDb-AO.

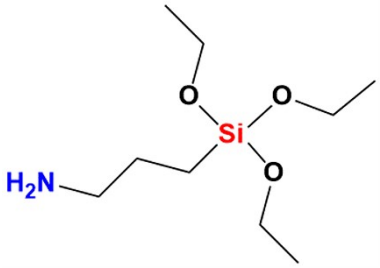

Fig. S11. The chemical structure of APTES.

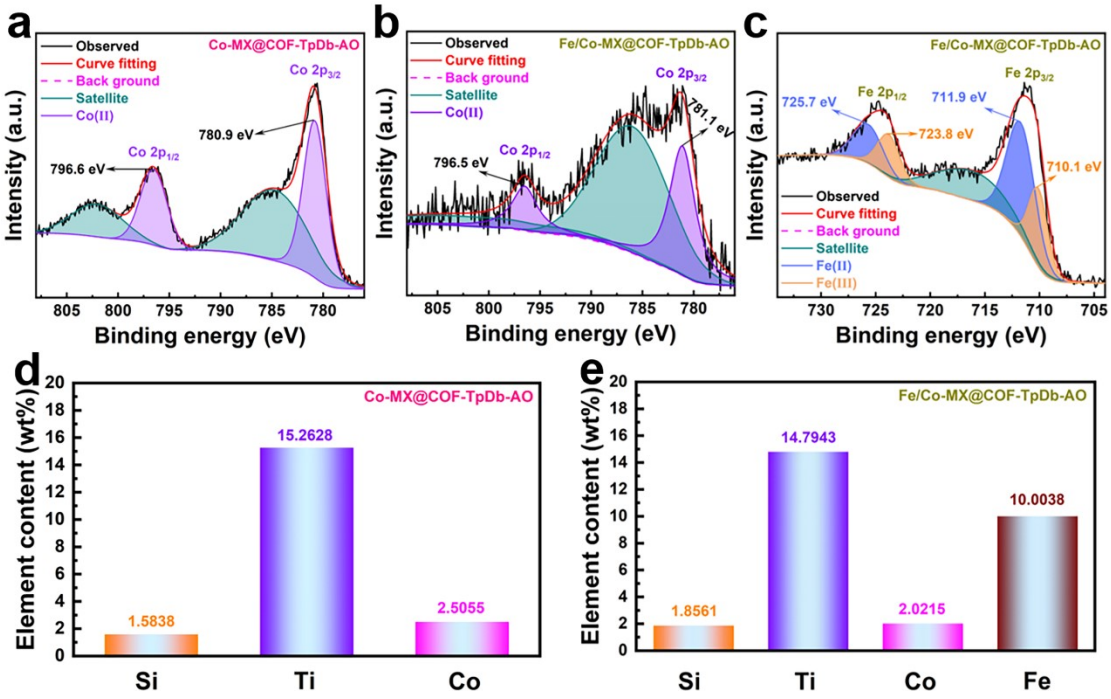

Fig. S12. (a) Co 2p XPS spectrum of Co-MX@COF-TpDb-AO. (b) Co 2p XPS spectrum of Fe/Co-MX@COF-TpDb-AO. (c) Fe 2p XPS spectrum of Fe/Co-MX@COF-TpDb-AO. (d) The element content in Co-MX@COF-TpDb-AO is analyzed by ICP-OES. (e) The element content in Fe/Co-MX@COF-TpDb-AO is analyzed by ICP-OES.

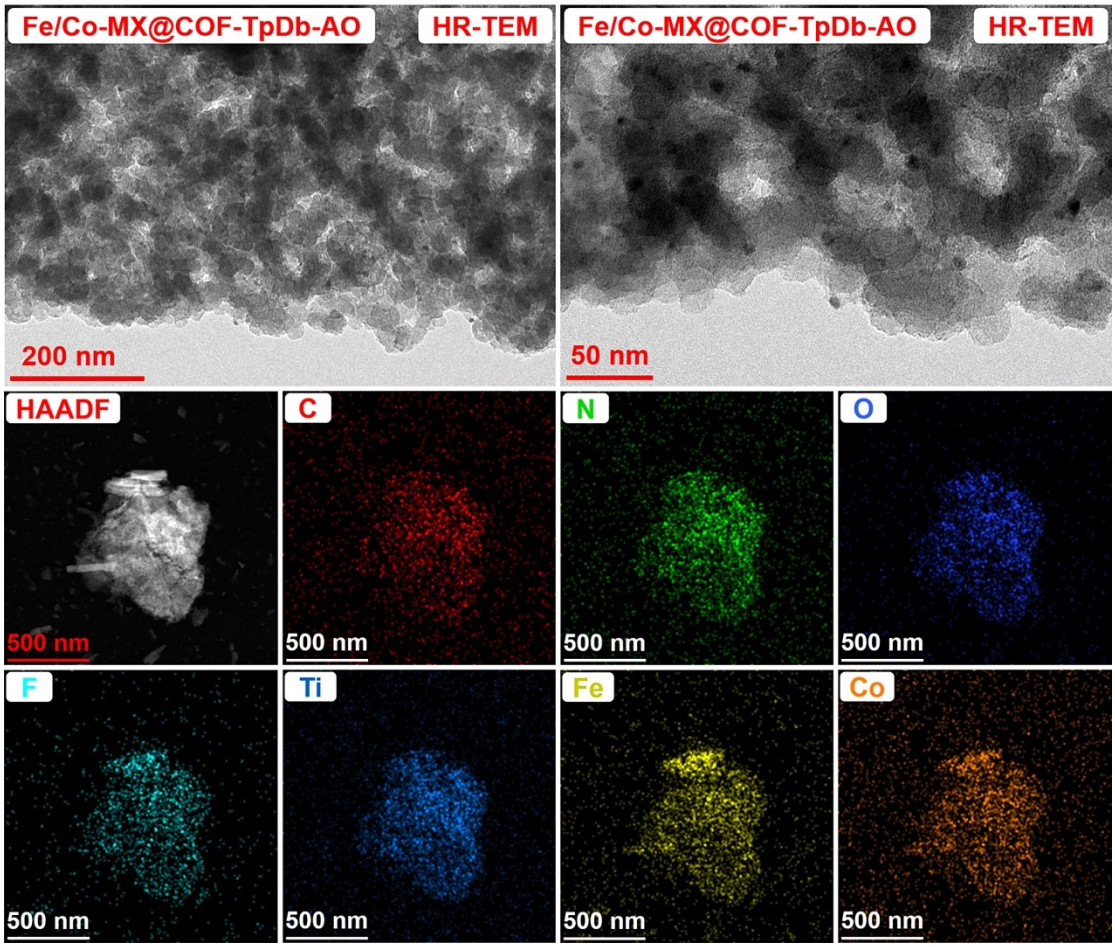

Fig. S13. HR-TEM images of Fe/Co-MX@COF-TpDb-AO and corresponding EDS mapping images of homogeneously distributed C, N, O, F, Ti, Fe, and Co.

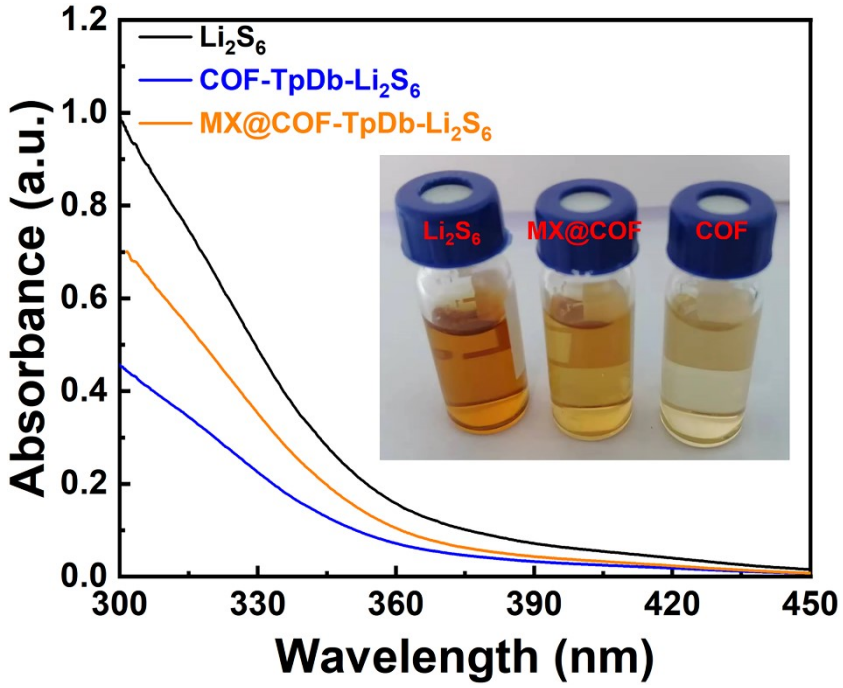

Fig. S14. UV-vis absorption spectra and Optical photographs of Li_2S_6 solutions containing different materials after resting for 6 h.

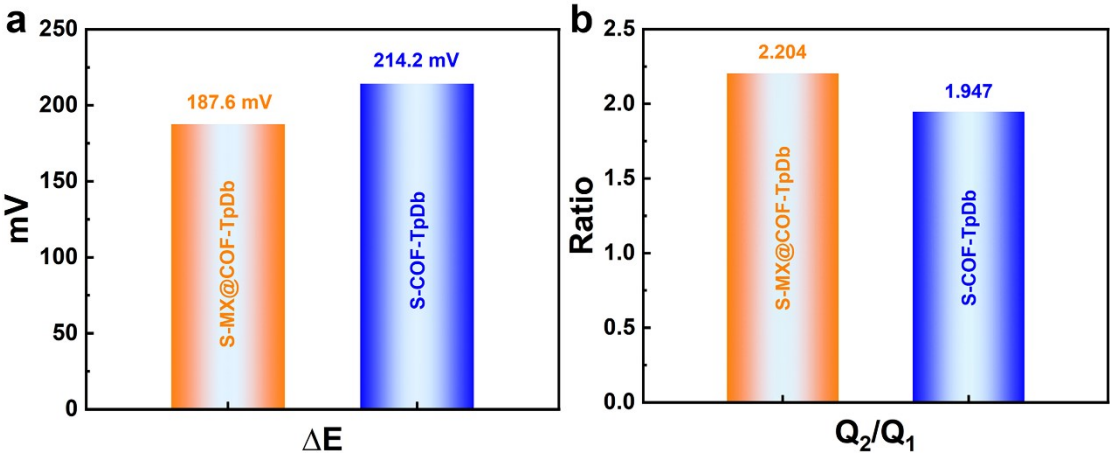

Fig. S15. Values of ΔE and Q_2/Q_1 obtained from the charge-discharge profiles of S-COF-TpDb and S-MX@COF-TpDb at 0.2 C.

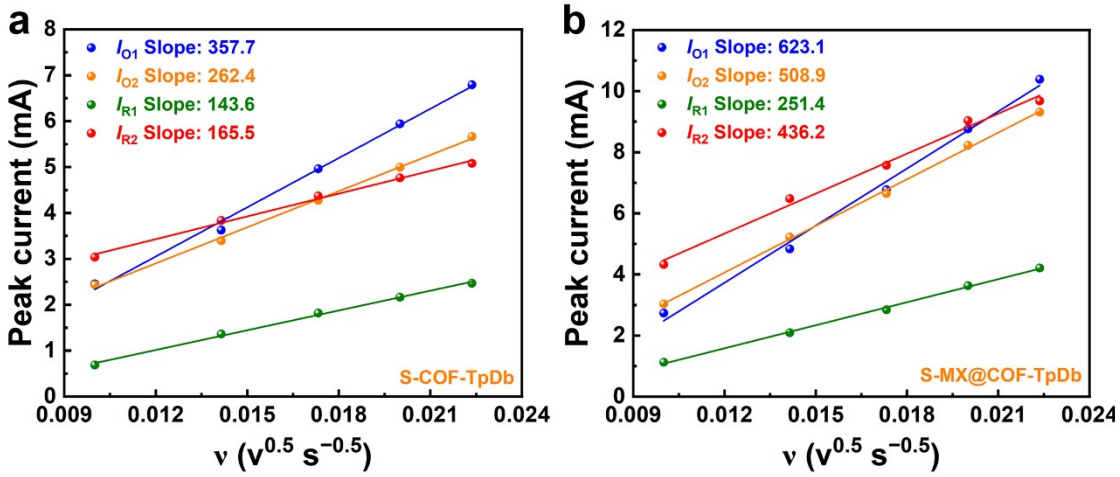

Fig. S16. Calculated Li^+ diffusion coefficients of (a) S-COF-TpDb and (b) S-MX@COF-TpDb modified batteries.

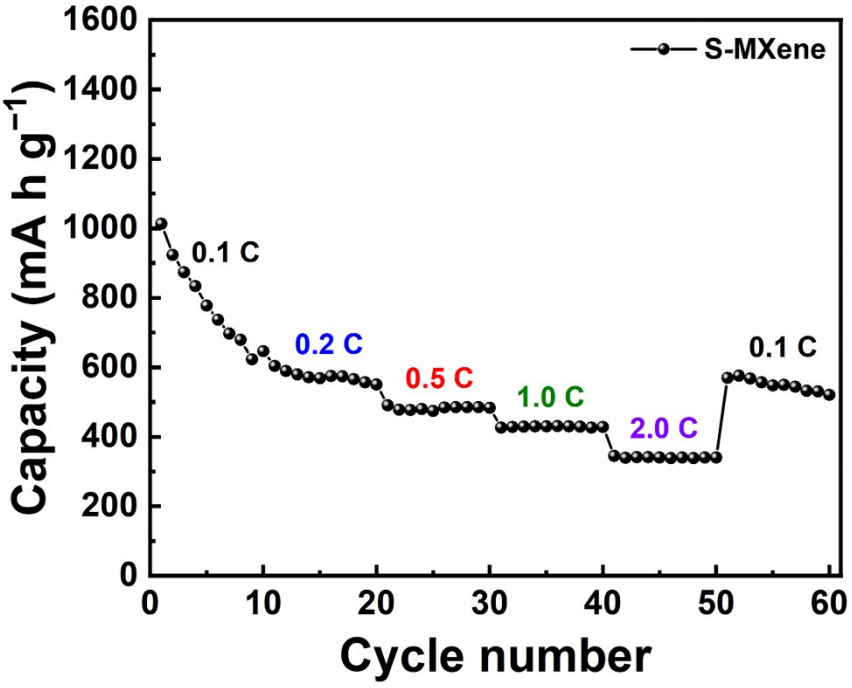

Fig. S17. Rate capability of S-MXene.

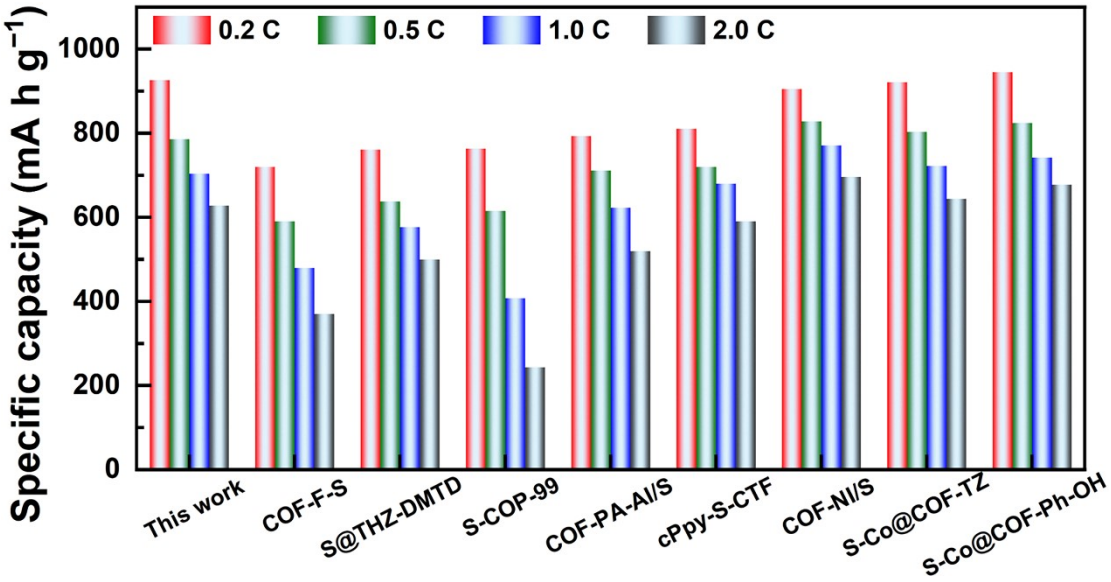

Fig. S18 Comparison rate performance of various COF-modified batteries.[S2–9]

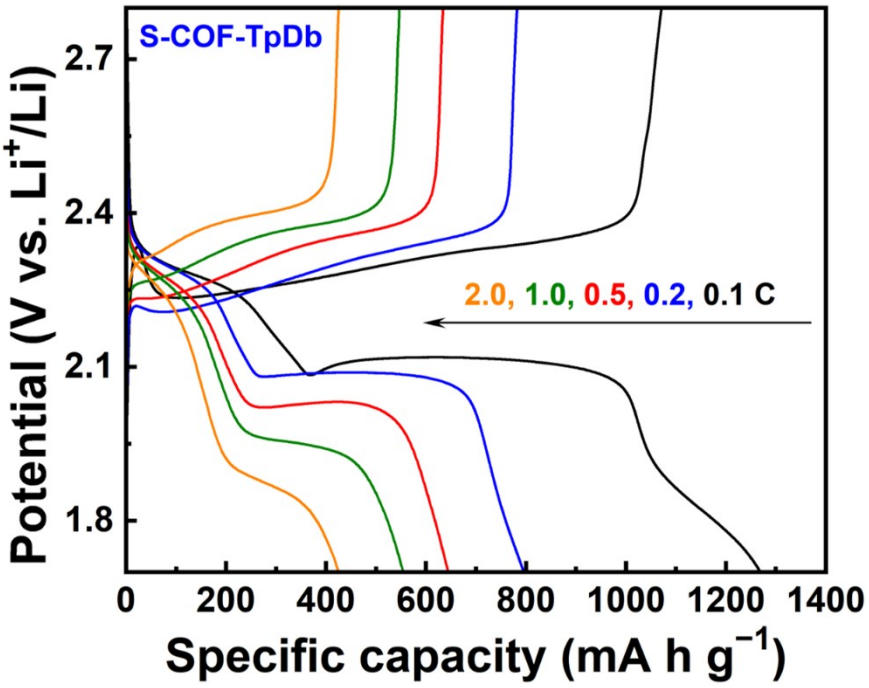

Fig. S19. Galvanostatic charge-discharge profiles of S-COF-TpDb modified battery at different rates.

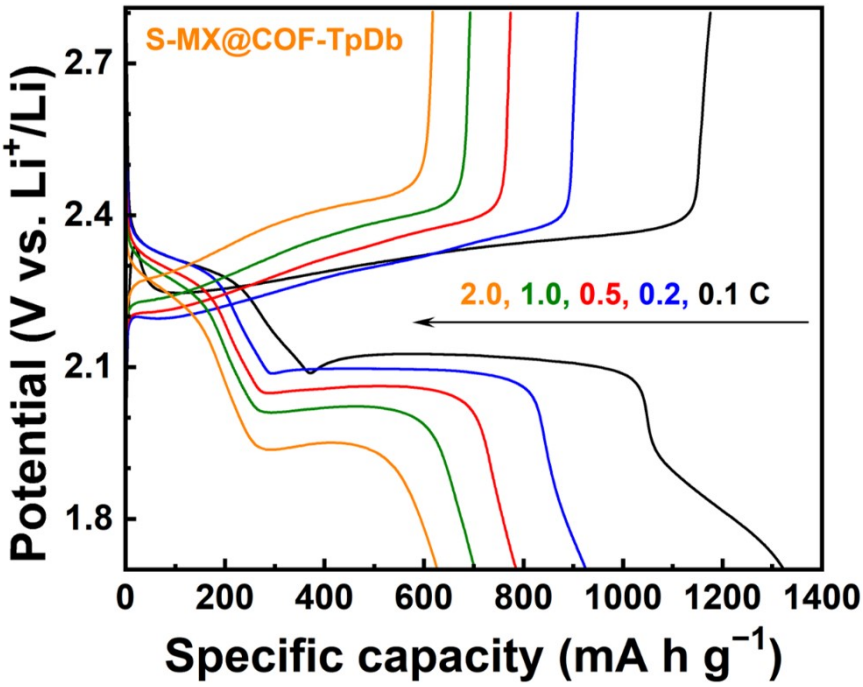

Fig. S20. Galvanostatic charge-discharge profiles of S-MX@COF-TpDb modified battery at different rates.

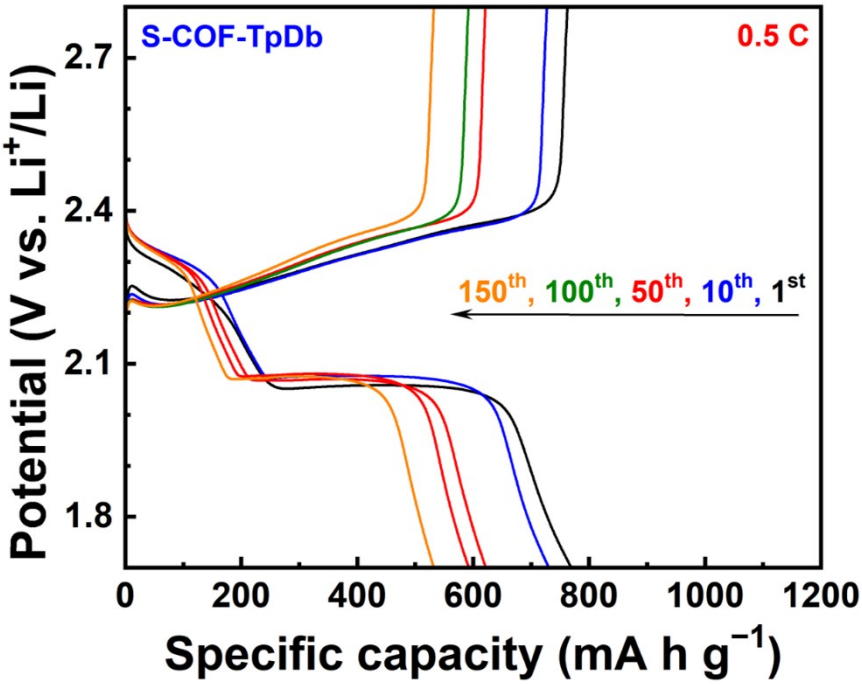

Fig. S21. Galvanostatic charge-discharge profiles of S-COF-TpDb modified battery at 0.5 C for different cycles.

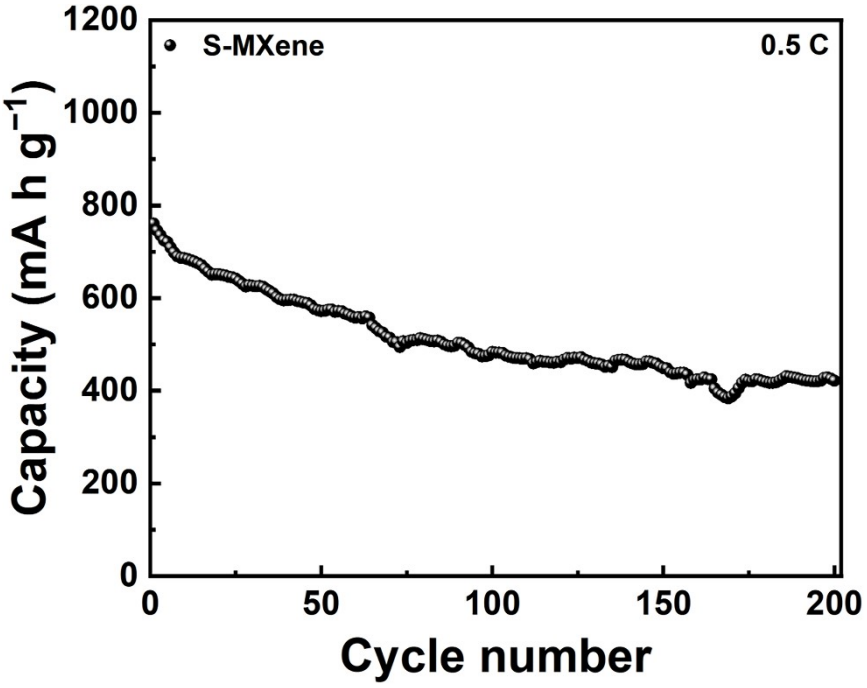

Fig. S22. Cycling capability of S-MXene modified battery at 0.5 C for 200 cycles.

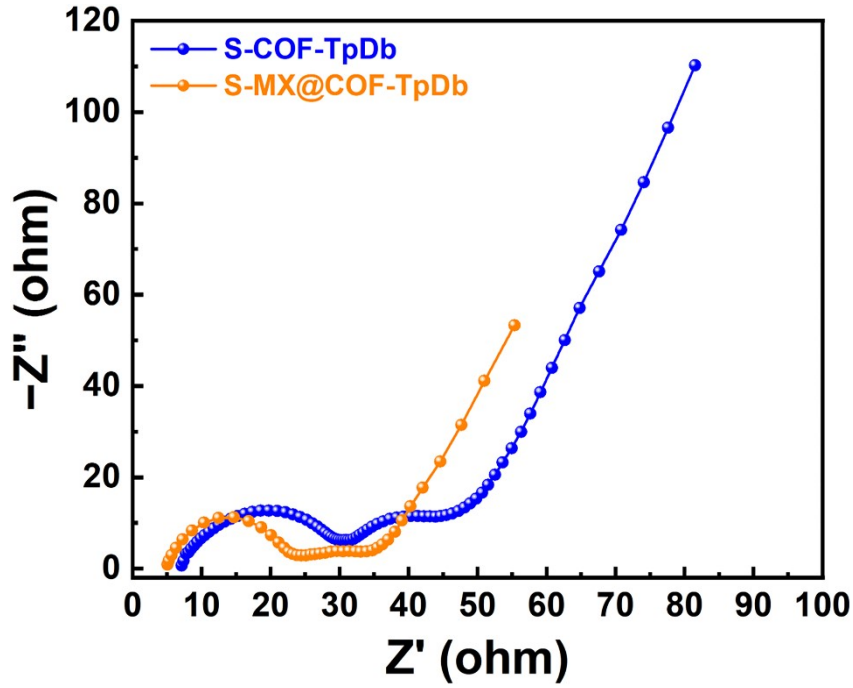

Fig. S23. EIS spectra of different COFs modified batteries after 300 cycles at 0.5 C.

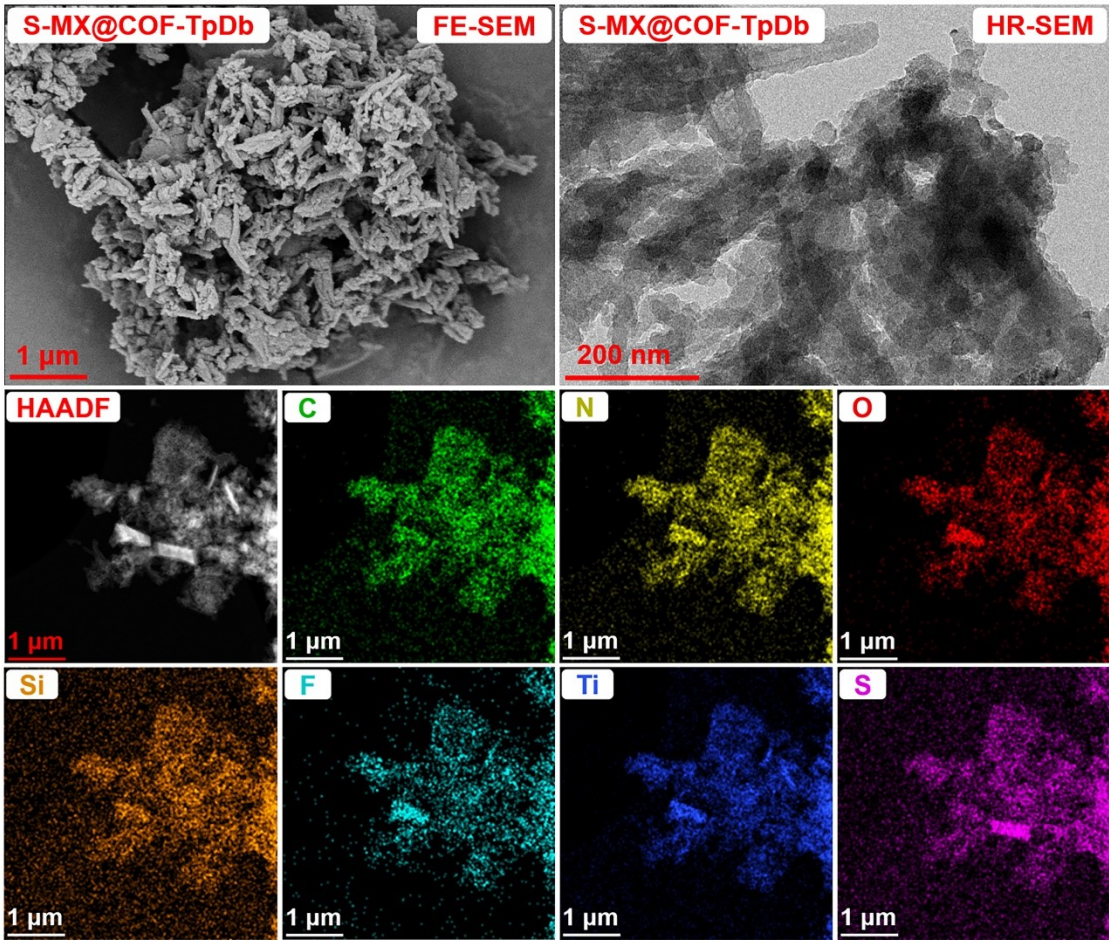

Fig. S24. After 300 cycles of Li-S battery testing, the FE-SEM and HR-TEM images of S-MX@COF-TpDb and corresponding EDS mapping images of homogeneously distributed C, N, O, Si, F, Ti, and S.

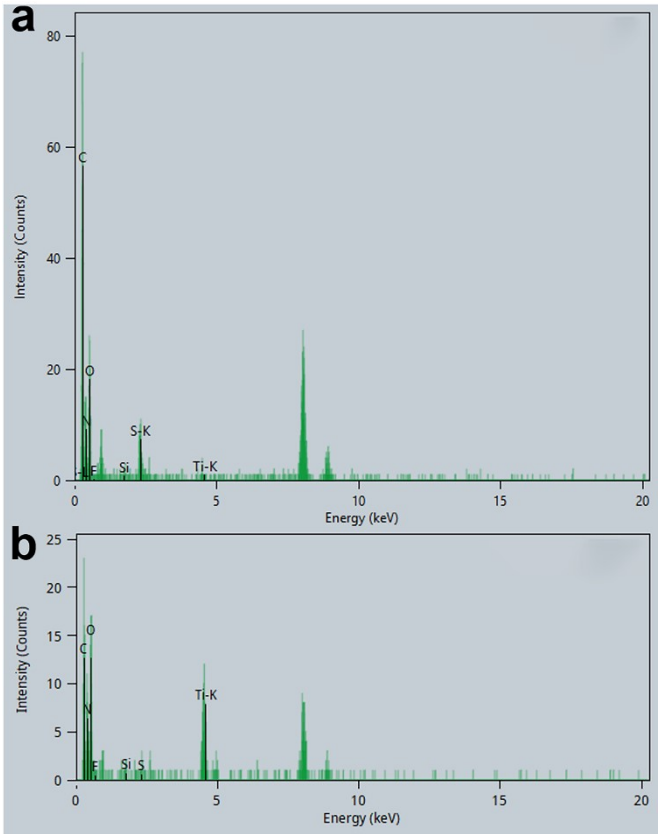

Fig. S25. EDS spectra of S-MX@COF-TpDb (a) before and (b) after 300 Li-S cycles.

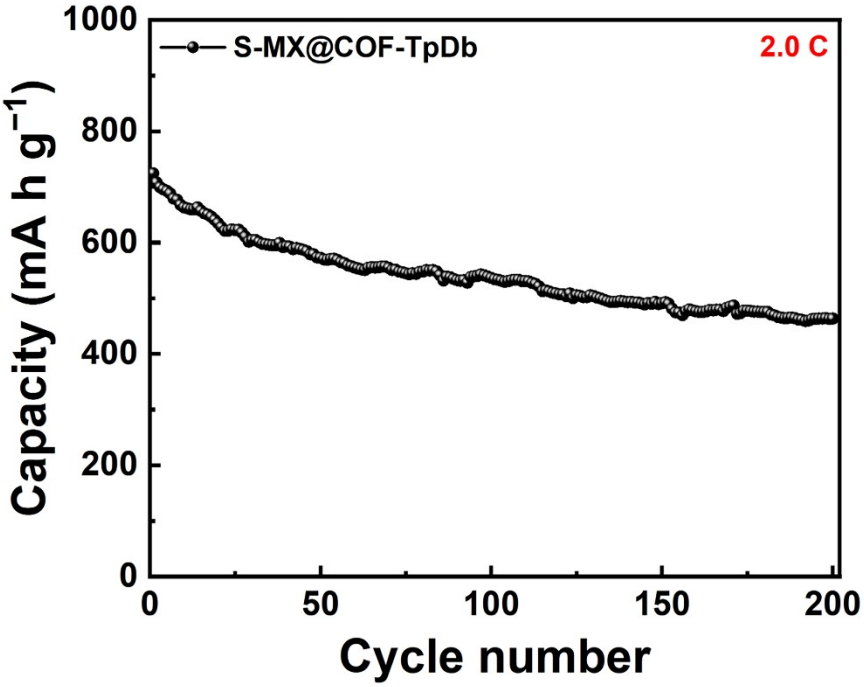

Fig. S26. Cycling capability of S-MX@COF-TpDb at 2.0 C for 200 cycles.

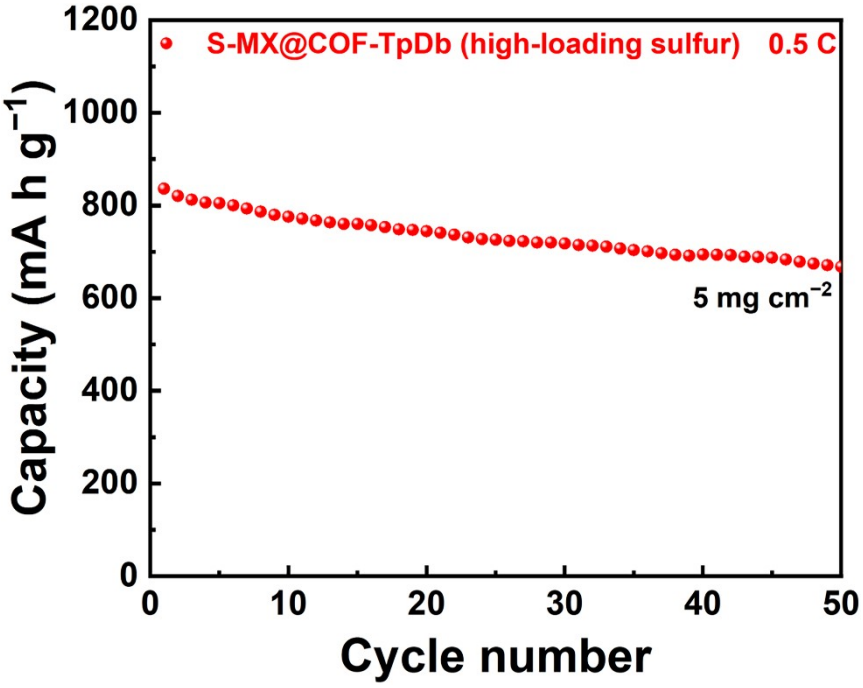

Fig. S27. Cycling capability of high-loading sulfur cathode (5 mg cm^{-2}) at 0.5 C for 50 cycles.

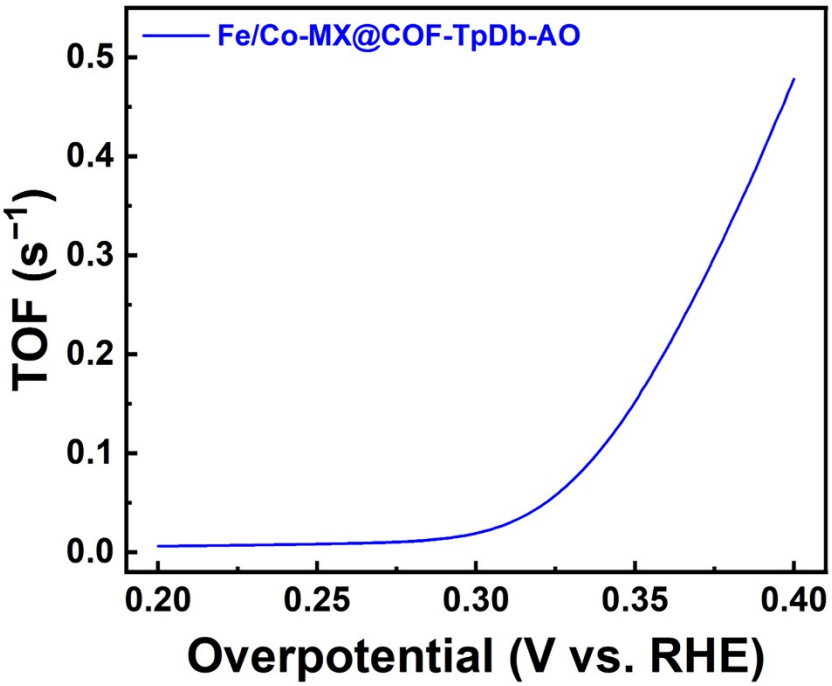

Fig. S28. TOF values of Fe/Co-MX@COF-TpDb-AO.

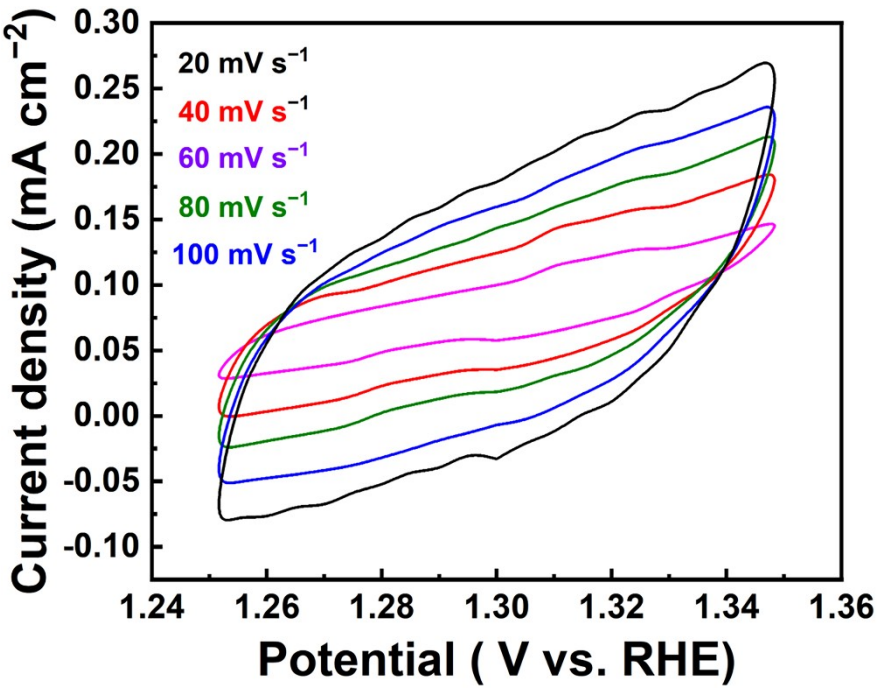

Fig. S29. CV curves of Fe/Co-MX@COF-TpDb-AO at different scan rates from 20 to 100 mV s^{-1}.

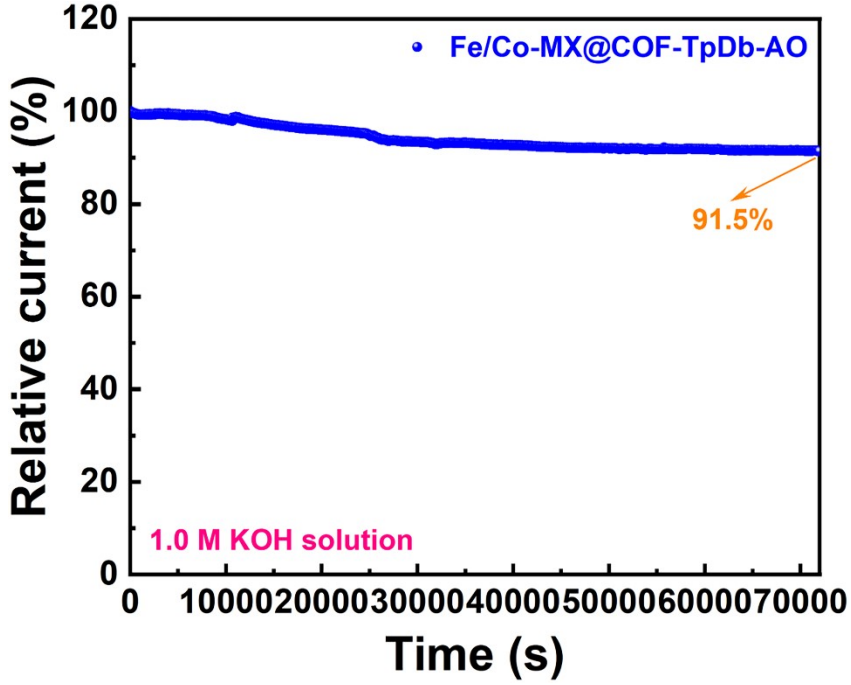

Fig. S30. *I*−*t* curve for Fe/Co-MX@COF-TpDb-AO after 72,000 s OER test.

Table S1. Charge transfer resistance (R_{ct}) of different catalysts.

Samples	R_{ct} [Ω]
MX@COF-TpDb-AO	1524
Fe-MX@COF-TpDb-AO	749.9
Co-MX@COF-TpDb-AO	520.9
Ni-MX@COF-TpDb-AO	758.3
Fe/Co-MX@COF-TpDb-AO	14.4
Fe/Ni-MX@COF-TpDb-AO	19.9
Co/Ni-MX@COF-TpDb-AO	159.6
Fe/Co/Ni-MX@COF-TpDb-AO	21.7

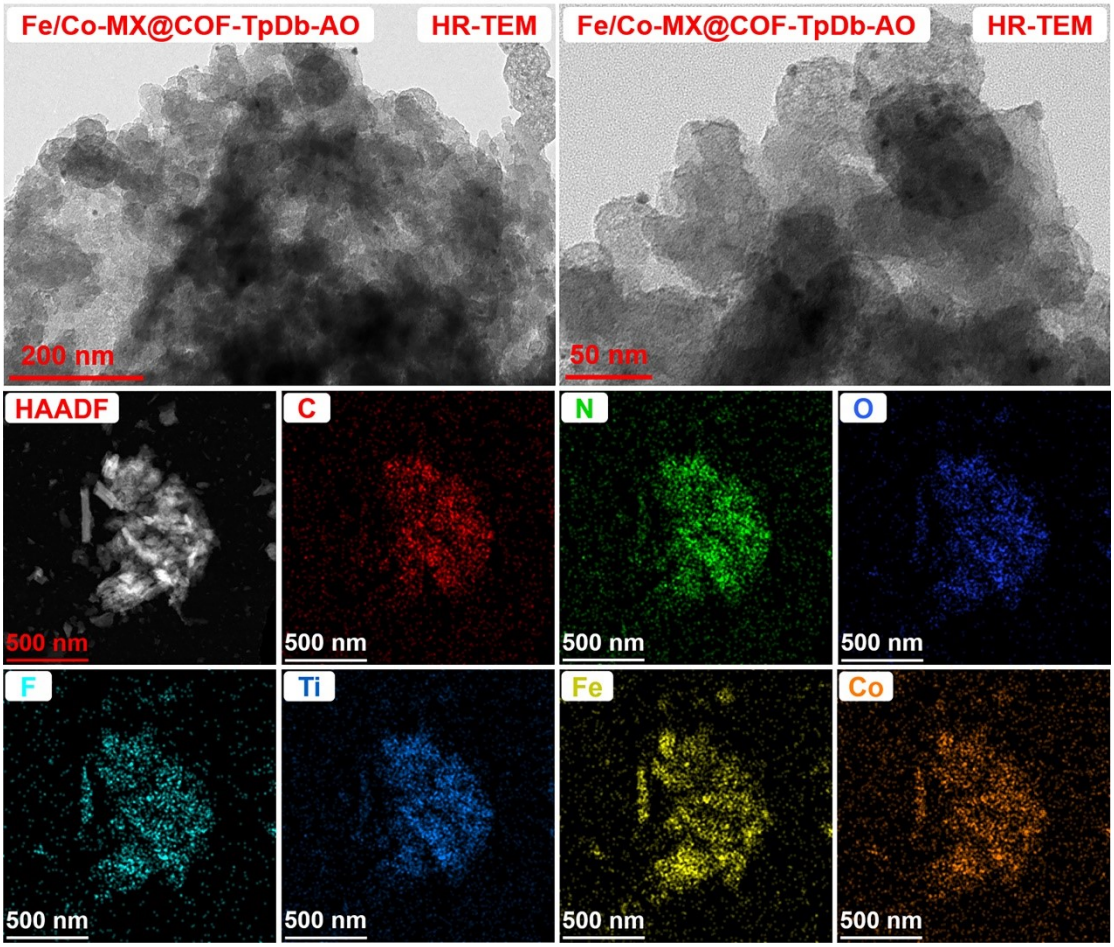

Fig. S31. HR-TEM and EDS-mapping images of Fe/Co-MX@COF-TpDb-AO after 1000 OER cycles.

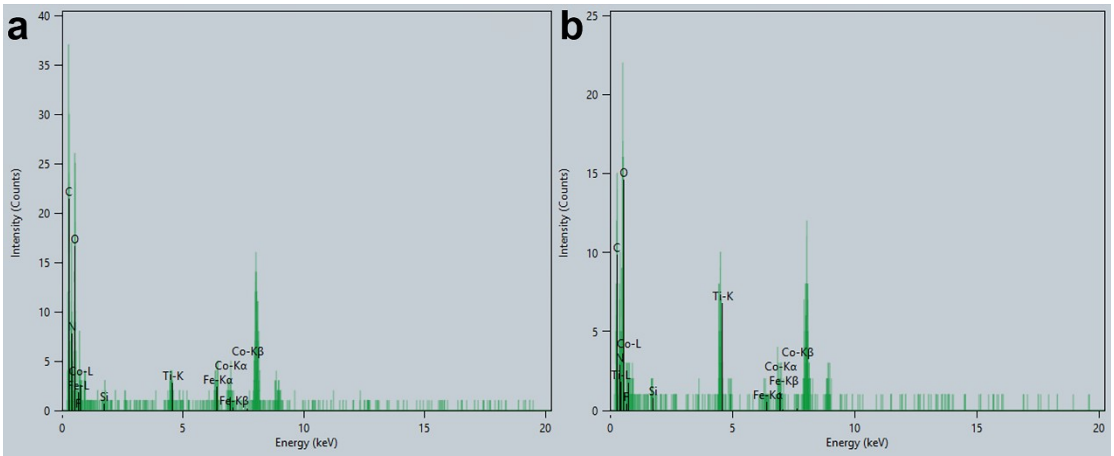

Fig. S32. EDS spectra of Fe/Co-MX@COF-TpDb-AO (a) before and (b) after 1000 OER cycles.

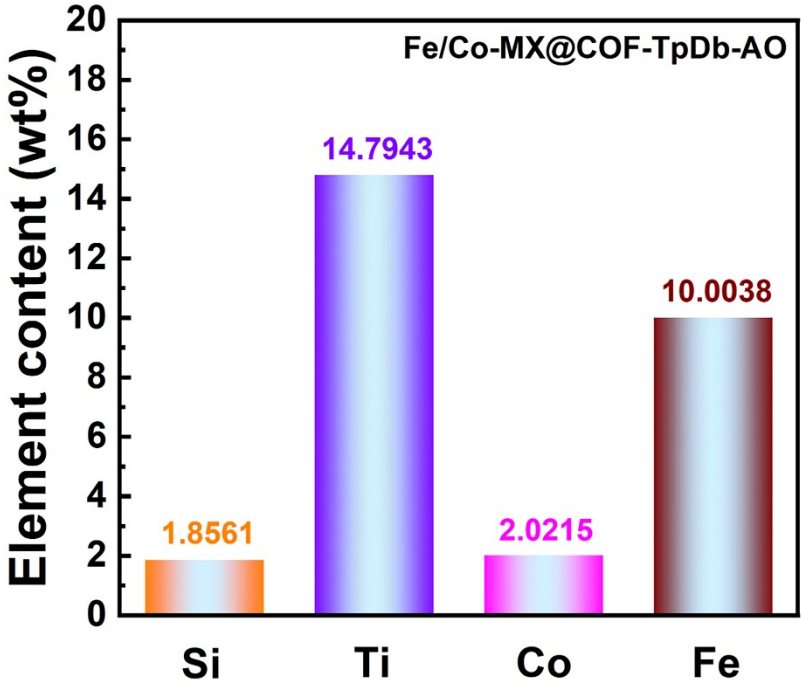

Fig. S33. After 72,000-second chronoamperometry test (OER), the elemental content of Fe/Co-MX@COF-TpDb-AO is analyzed by ICP-OES.

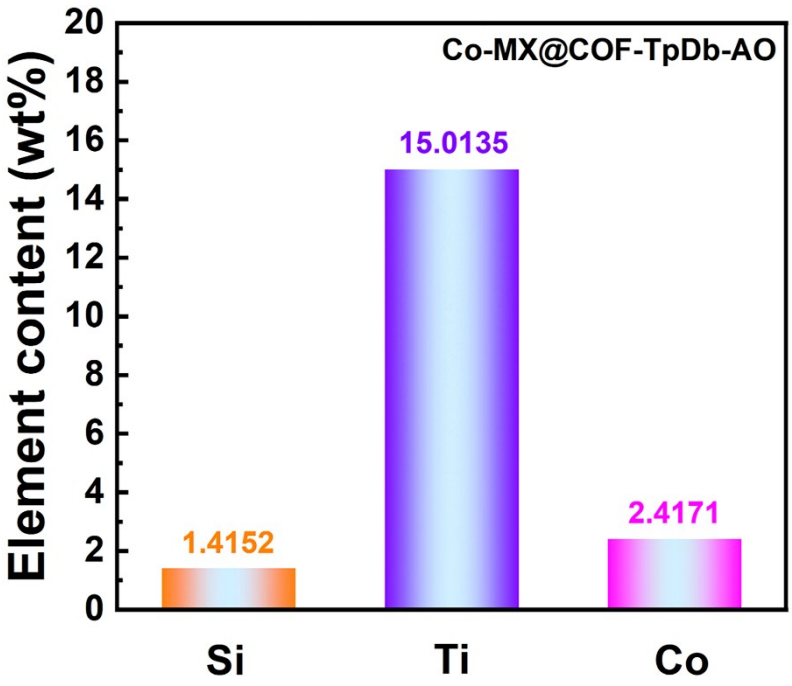

Fig. S34. After 1000 CV cycles (ORR), the elemental content of Co-MX@COF-TpDb-AO is analyzed by ICP-OES.

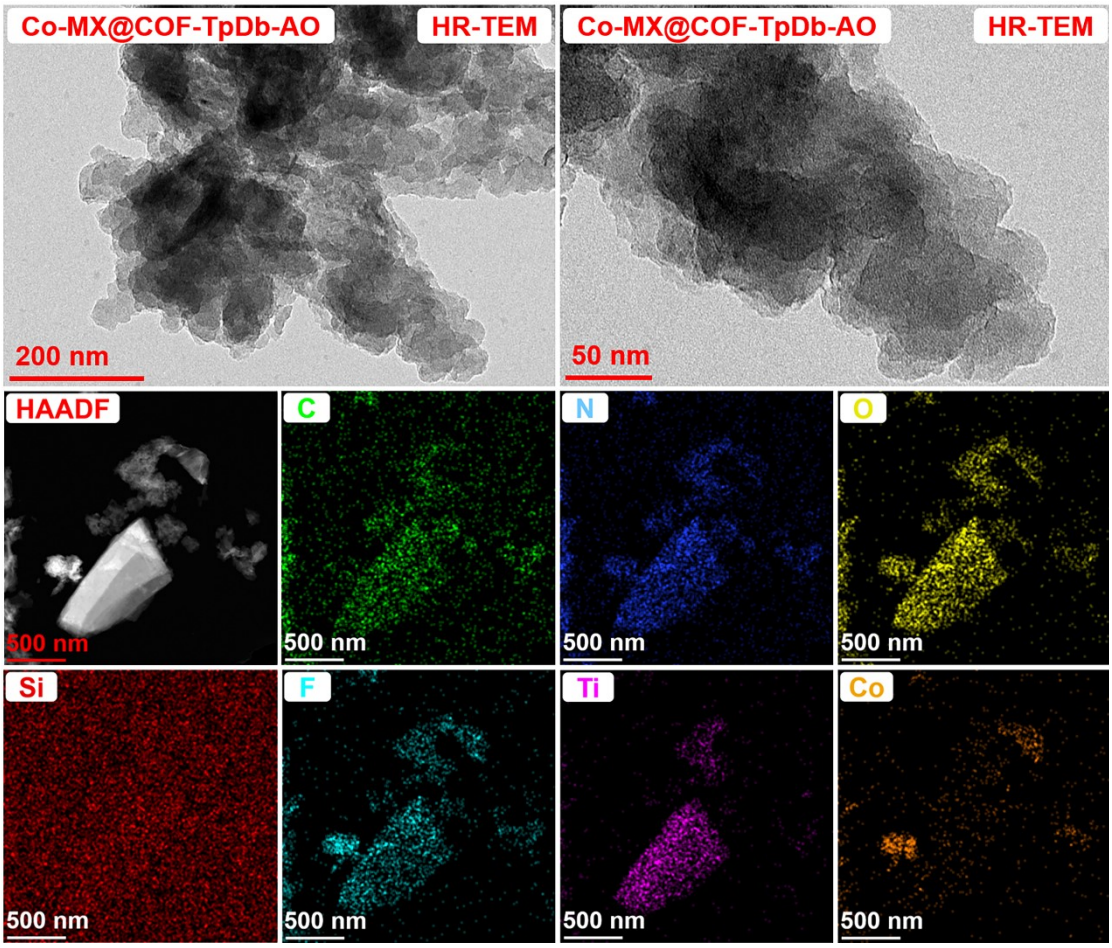

Fig. S35. HR-TEM and EDS-mapping images of Co-MX@COF-TpDb-AO after 1000 ORR cycles.

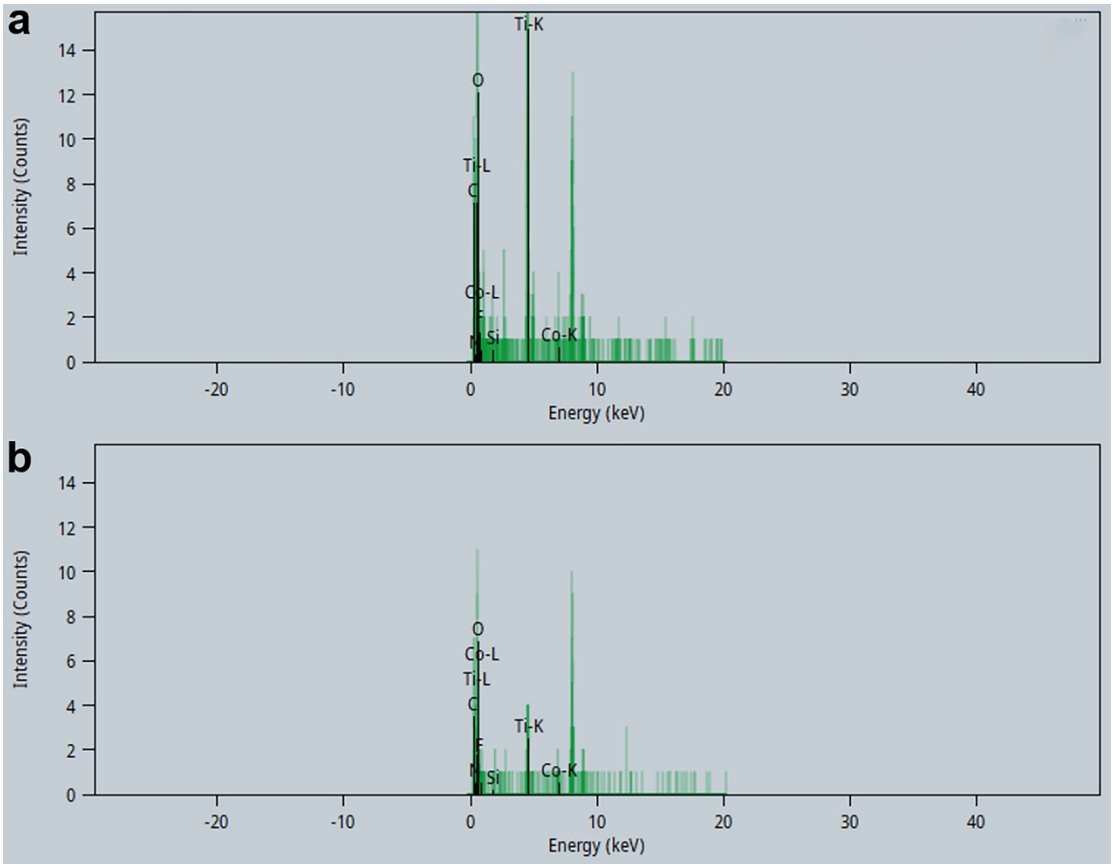

Fig. S36. EDS spectra of Co-MX@COF-TpDb-AO (a) berore and (b) after 1000 ORR cycles.

References

[S1] Q. Sun, B. Aguila, L. D. Earl, C. W. Abney, L. Wojtas, P. K. Thallapally and S. Ma, Covalent organic frameworks as a decorating platform for utilization and affinity enhancement of chelating sites for radionuclide sequestration, *Adv. Mater,* **2018**, *30*, 1705479.

[S2] D. Wang, N. Li, Y. Hu, S. Wan, M. Song, G. Yu, Y. Jin, W. Wei, K. Han, G. Kuang and W. Zhang, Highly fluoro-substituted covalent organic framework and its application in lithium-sulfur batteries, *ACS Appl. Mater. Interfaces,* **2018**, *10*, 42233−42240.

[S3] R. Yan, B. Mishra, M. Traxler, J. Roeser, N. Chaoui, B. Kumbhakar, J. Schmidt, S. Li, A. Thomas and P. Pachfule, A thiazole-linked covalent organic framework for lithium-sulphur batteries, *Angew. Chem. Int. Ed.,* **2023**, *62*, e202302276.

[S4] H. Shin, D. Kim, H. J. Kim, J. Kim, K. Char, C. T. Yavuz and J. W. Choi, Fluorinated covalent organic polymers for high performance sulfur cathodes in lithium-sulfur batteries, *Chem. Mater.,* **2019**, *31*, 7910−7921.

[S5] X. Liu, M. Xia, Y. Zhao, T. Xia, Y. Li, J. Xiao, Z. Sui and Q. Chen, Cationic covalent organic framework via cycloaddition reactions as sulfur-loaded matrix for lithium-sulfur batteries, *Mater. Today Chem.,* **2022**, *23*, 100664.

[S6] J. Kim, A. Elabd, S. Chung, A. Coskun and J. W. Choi, Covalent triazine frameworks incorporating charged polypyrrole channels for high-performance lithium-sulfur batteries, *Chem. Mater.,* **2020**, *32*, 4185−4193.

[S7] S. Wang, Y. Liang, T. Dai, Y. Liu, Z. Sui, X. Tian and Q. Chen, Cationic

covalent-organic framework for sulfur storage with high-performance in lithium-sulfur batteries, *J. Colloid Interface Sci.,* **2021**, *591*, 264−272.

[S8] Z. Wu, J. Luo, Y. Liang, X. Yu, Y. Zhao, Y. Li, W. Wang, Z. Sui, X. Tian, Q. Chen, Tetrazole-functionalized benzoquinoline-linked covalent organic frameworks with efficient performance for electrocatalytic H_2O_2 production and Li-S batteries, *Mater. Chem. Front.,* **2023**, *7*, 1650−1658.

[S9] Z. Wu, L. Feng, J. Luo, Y. Zhao, X. Yu, Y. Li, W. Wang, Z. Sui, X. Tian and Q. Chen, Metalation of functionalized benzoquinoline-linked COFs for electrocatalytic oxygen reduction and lithium-sulfur batteries, *J. Colloid Interface Sci.,* **2023**, *650*, 1466−1475.